

## ANALYSIS OF NEAR-SOURCE STATIC AND DYNAMIC MEASUREMENTS FROM THE 1979 IMPERIAL VALLEY EARTHQUAKE

BY RALPH J. ARCHULETA

### ABSTRACT

Gross features of the rupture mechanism of the 1979 Imperial Valley earthquake ( $M_L = 6.6$ ) are inferred from qualitative analysis of near-source ground motion data and observed surface rupture. A lower bound on the event's seismic moment of  $2.5 \times 10^{25}$  dyne-cm is obtained by assuming that the average slip over the whole fault plane equals the average surface rupture, 40.5 cm. Far-field estimates of moment suggest an average slip over the fault plane of 105 cm, from which a static stress drop of 11 bars is obtained. An alternative slip model, consistent with the far-field moment, has 40.5 cm of slip in the upper 5 km of the fault and 120 cm of slip in the lower 5 km. This model suggests a static stress drop of 39 bars. From the lower estimate of 11 bars, an average strain drop of 32  $\mu$ strain is derived. This strain drop is four times greater than the strain that could have accumulated since the 1940 El Centro earthquake based on measured strain rates for the region. Hence, a major portion of the strain released in the 1979 main shock had been accumulated prior to 1940.

Unusually large amplitude (500 to 600 cm/sec<sup>2</sup>) vertical accelerations were recorded at stations E05, E06, E07, E08, EDA of the El Centro array, and the five stations of the differential array near EDA. Although the peak acceleration of 1705 cm/sec<sup>2</sup> at E06 is probably amplified by a factor of 3 due to local site conditions, these large amplitude vertical accelerations are unusual in that they are evident on only a few stations, all of which are near the fault trace and at about the same epicentral range. Two possible explanations are considered: first, that they are due to a direct P wave generated from a region about 17 km north of the hypocenter, or second, that they are due to a PP phase that is unusually strong in the Imperial Valley due to the large P-wave velocity gradient in the upper 5 km of the Imperial Valley.

Based on the distribution of both the horizontal and vertical offsets, it is likely that the rupture went beyond stations E06 and E07 during the main shock. By exploiting the antisymmetry of the parallel components of particle velocity between E06 and E07 and by examining polarization diagrams of the particle velocity at E06 and E07, an average rupture velocity in the basement of 2.5 to 2.6 km/sec between the hypocenter and station E06 is obtained. In addition, several lines of evidence suggest that the Imperial fault dips about 75° to the NE.

### INTRODUCTION

The 15 October 1979 Imperial Valley earthquake in southeastern California and northern Baja Mexico (Figure 1) has provided the most complete set of near- and far-field data for a damaging earthquake to date. More than 40 strong motion instruments in the United States (Brady *et al.*, 1980) and in Mexico (Brune *et al.*, 1982) recorded the near-source ground acceleration at distances less than 35 km from the Imperial fault. The right-lateral horizontal offsets and the vertical offsets were measured within days of the main shock (Sharp *et al.*, 1982). A coseismic strain offset was recorded by three laser strainmeters at Pinon Observatory about 130 km from the epicenter (Wyatt, 1980). Throughout the world, the  $M_L = 6.6$  (Chavez *et*

*al.*, 1982) main shock was well recorded on long-period seismometers (Julian *et al.*, 1982). Since the main shock was well recorded both near and far and over the entire seismic frequency band, the Imperial Valley earthquake provides an extraordinary opportunity for studying the earthquake mechanism from many different viewpoints. My approach in this paper is to examine the near-field static measurements

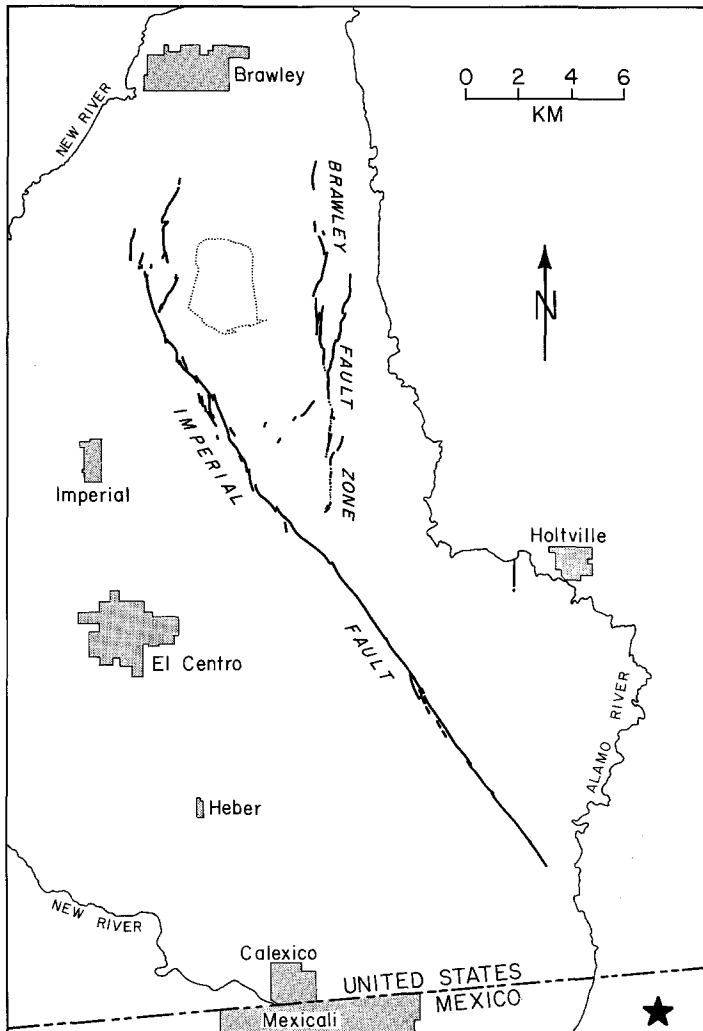


FIG. 1. Region of southeastern California and northern Baja Mexico directly affected by the main shock. Surface traces of the Imperial fault, striking NNW, and the Brawley fault, striking north, on which surface rupture was measured are shown. Star marks epicenter.

and the strong motion particle acceleration and velocity. It is not my intention to conclude with a detailed description of the faulting process, but rather to provide a framework from which future investigations can be initiated.

#### LOCAL SETTING

Study of the Imperial Valley earthquake has been immensely facilitated by detailed knowledge of the *P*-wave velocity ( $V_p$ ) structure of the Imperial Valley region obtained by Fuis *et al.* (1982) and McMechan and Mooney (1980). In general,

at any point in the valley, the velocity profile can be broken into three regions as shown in Figure 2. The shallowest region, the "sediments," is characterized by large velocity gradients. It overlies a more uniform "basement" which in turn is separated from the faster underlying "subbasement" by a velocity discontinuity. The sediment and basement thicknesses vary substantially throughout the valley, and the  $P$ -wave velocity profile shown in Figure 2 is that obtained by McMechan and Mooney (1980) along a line nearly parallel to the Imperial fault and 10 km east of it. Velocity structure also varies across the Imperial fault, with the west side of the fault being as much as 0.5 km/sec faster than the east side (Fuis *et al.*, 1982).

The  $S$ -wave velocity ( $V_s$ ) structure shown in Figure 2 was derived from the study of aftershocks of the Imperial Valley main shock (Archuleta *et al.*, 1979) and drill logs in the Imperial Valley (Shannon *et al.*, 1976). The  $V_p/V_s$  ratio monotonically

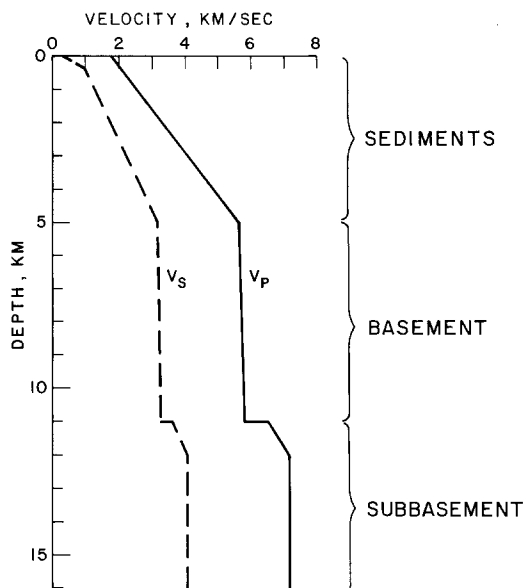


FIG. 2. Vertical profiles of  $S$ - ( $V_s$ ) and  $P$ -wave ( $V_p$ ) velocity structures in the Imperial Valley with structural nomenclature.

decreases from 9.0 at the surface to 2.13 at 0.35 km. From 0.35 to 5 km, the ratio decreases from 2.13 to 1.78. From 5 to 11 km, the ratio is held constant at 1.78, a value appropriate for oceanic crustal material. Below 11 km, the Poisson solid value of 1.73 is used.

To illustrate some of the principal phases that are discussed later, I show in Figure 3 travel-time curves for point sources located at 4.0 and 8.0 km depth, respectively. The labeled branches of the travel-time curves are shown schematically in the insets. I follow a nomenclature system similar to that used for teleseismic phases with  $p$  and  $s$  denoting  $P$  and  $S$  waves that are traveling upward from the source, and  $P$  and  $S$  denoting waves traveling downward from the source. Of particular note are the families of free-surface reflected phases  $PP$  and  $PPP$ . Because of the strong velocity gradient in the top 5 km of the Imperial Valley, these phases were observed at much smaller epicentral distances than usual, and were quite large in the refraction profiles of McMechan and Mooney (1980) and Fuis *et al.* (1982). For buried sources, these phases have large amplitudes at the cusps of

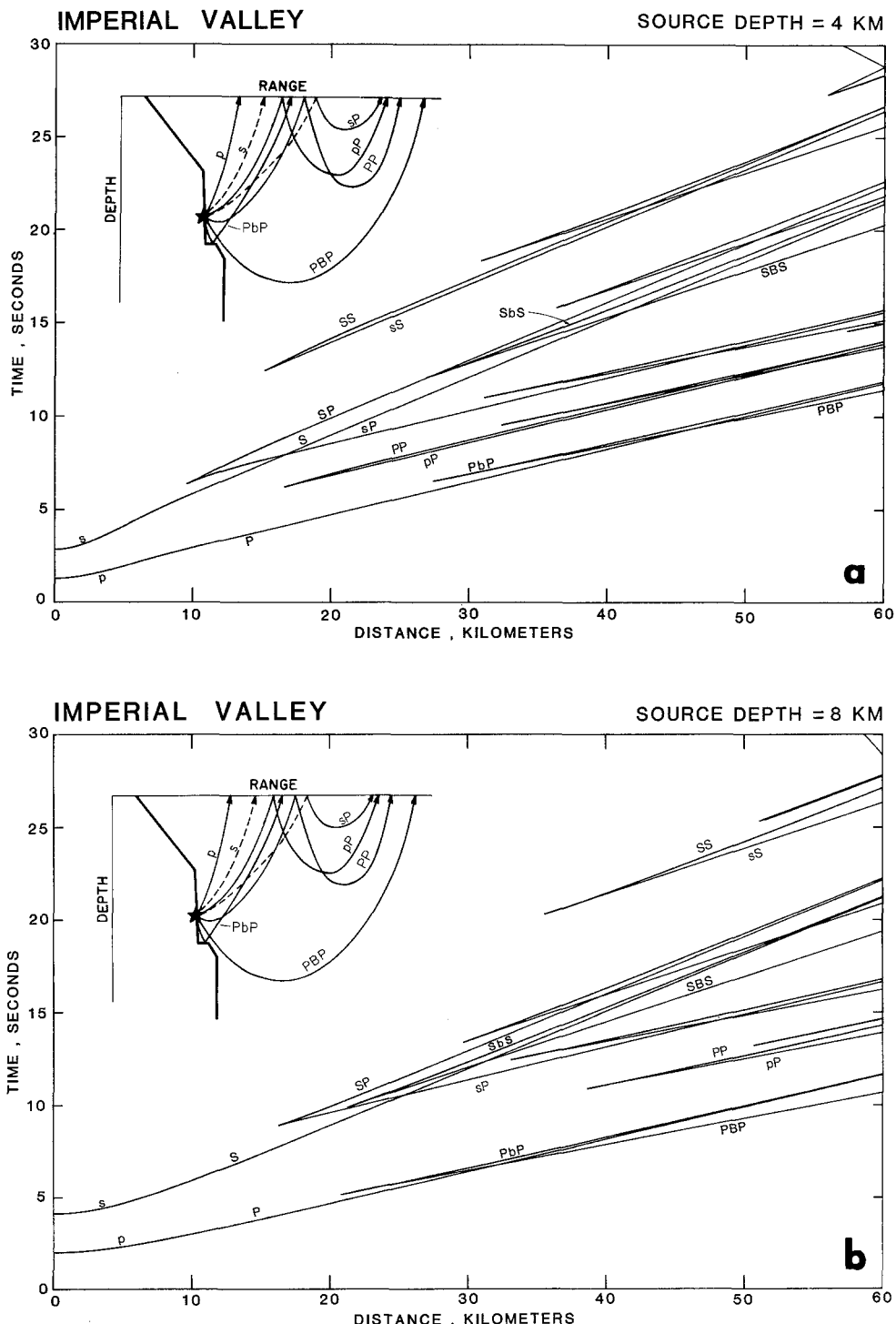


FIG. 3. Travel-time curves for the Imperial Valley assuming a flat-layered velocity structure based on Figure 2. Phases shown are  $P$ ,  $PP$ ,  $S$ ,  $SS$ , the reflections from the 6.6 km/sec discontinuity, and  $S$  to  $P$  conversions. The inset is a schematic representation of geometrical ray paths from point source (star).

(a) Source is at 4.0 km depth. (b) The source is at 8.0 km depth.

their travel-time curves, i.e., at the epicentral distances where  $pP$  and  $PP$ , or  $sS$  and  $SS$ , merge. Because the time separation between the  $pP$  and  $PP$  arrivals is so small, I will use the term “ $PP$ ” to refer to the combined arrival.

Several lines of evidence suggest that the Imperial fault is not vertical. First, the hypocenter determined by Archuleta (1982) (Figure 1) is east of the fault and implies a dip of  $82^\circ$ NE. (His hypocenter,  $32^\circ 39.50'N$ ,  $115^\circ 19.80'W$ , 8.0 km depth and 23:16:54.4 UTC origin time, is used throughout this paper.) From their refraction profiles, Fuis *et al.* (1982) noted basement offsets beneath the Imperial fault which lead to dips of  $70^\circ$ NE on the southeast end and  $78^\circ$ NE on the northwest end of the Imperial fault. Johnson (1979) finds that earthquakes with  $M_L \geq 3.0$  have epicenters that lie 2 to 3 km east of the fault, which lead to dip estimates of  $67^\circ$  to  $76^\circ$ NE if a hypocentral depth range of 6 to 10 km is assumed. From these, I have assumed that the average dip of the Imperial fault is  $75^\circ$ NE. This dip has an important effect on near-source ground motions.

#### LOCAL STRONG MOTION DATA

An extensive set of three-component accelerograms from the Imperial Valley earthquake was recorded in the United States by Brady *et al.* (1980) of the U.S. Geological Survey and McJunkin and Ragsdale (1980) of the California Division of Mines and Geology. The three components of particle acceleration are shown in Figures 4, 5, and 6. Positive vertical motion is up. The horizontal components are oriented parallel (positive motion along an azimuth  $140^\circ$  clockwise from north) and perpendicular (positive motion along the  $230^\circ$  azimuth) to the strike of the Imperial fault. Each figure shows the accelerometer sites, their three-letter station codes (Switzer *et al.*, 1981), and their recorded seismogram superposed on a base map of the northwest-trending Imperial fault, the north-striking Brawley fault, and the Archuleta (1982) epicenter. Only the first 10 sec of acceleration are shown. Table 1 gives station coordinates, trigger times, azimuth between station and epicenter, and epicentral distances.

The preeminent aspect of the vertical accelerations in Figure 4 is the  $1705\text{ cm/sec}^2$  peak ground acceleration (PGA) at station E06. The true PGA may be even larger than this once the instrument response is accounted for (Raugh, 1981). Although the large amplitude at E06 dominates, stations E05, E07, E08, and EDA also show peak vertical accelerations of 500 to  $600\text{ cm/sec}^2$ . At E06, the amplitude is increased by a factor of about 3 with respect to E07 (Mueller and Boore, 1981) due to local site conditions; if one corrects for the site amplification, the PGA at E06 is approximately the same as those at E05, E07, E08, and EDA. These large accelerations are unusual in that they appear on vertical rather than horizontal components; they are found on only stations which are at approximately the same epicentral range and close to the fault; they are near a node for  $P$ -wave radiation from a vertical fault and precede the arrival of the direct  $S$  waves from the hypocenter. Later, I examine possible causes for these vertical accelerations.

The horizontal components of acceleration (Figures 5 and 6) are characterized by their long periods that signal the arrival of the first  $S$  waves from the hypocenter. The maximum horizontal acceleration,  $794\text{ cm/sec}^2$ , occurs on the  $230^\circ$  component at Bonds Corner (BCR) almost 7 sec after triggering.

The particle velocity time histories (the first 30 sec) obtained by integrating (Brady *et al.*, 1980) the vertical,  $230^\circ$ , and  $140^\circ$  components of acceleration are shown in Figures 7, 8, and 9, respectively. In terms of amplitude alone, the  $230^\circ$

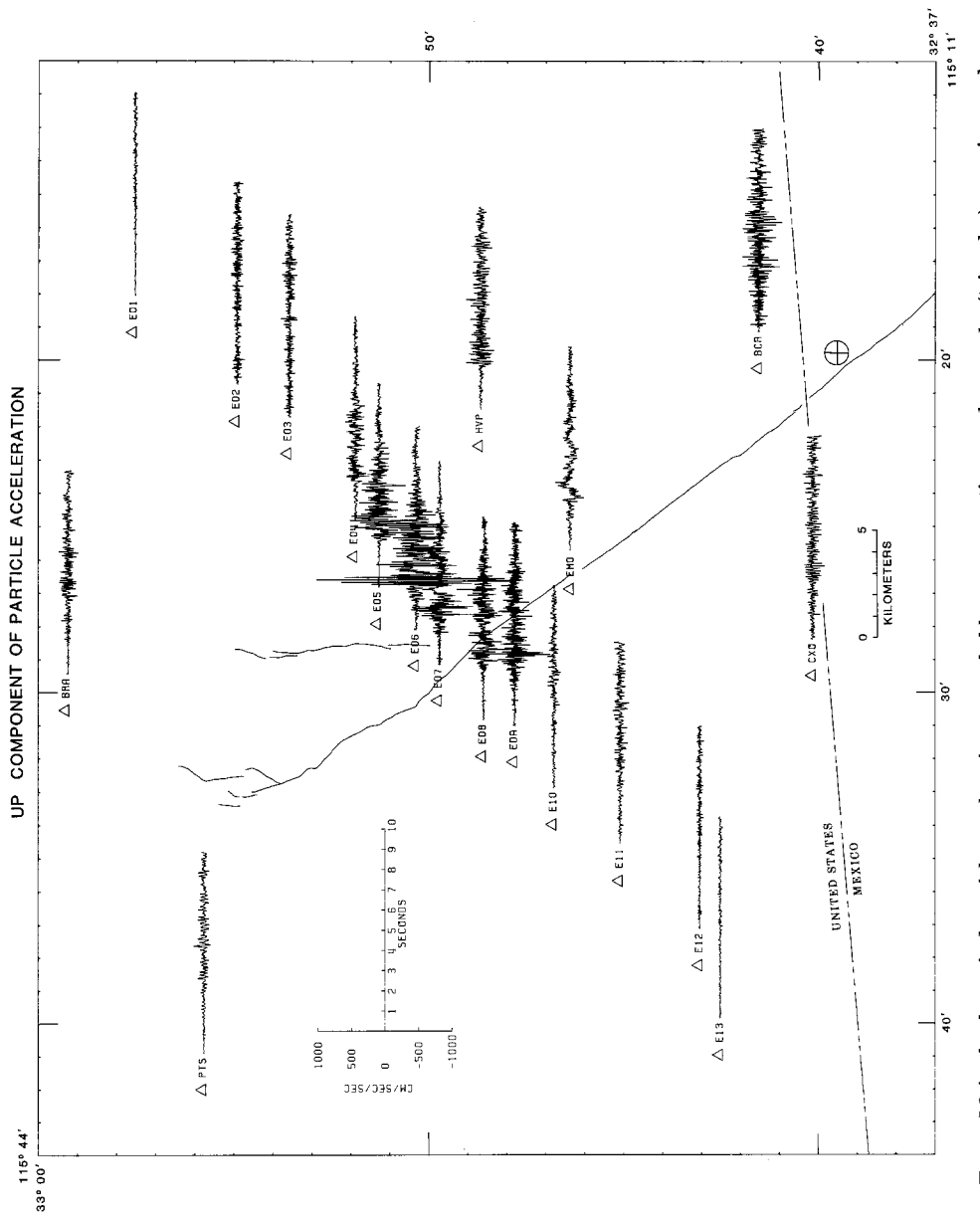


FIG. 4. Main shock vertical particle accelerations recorded by strong motion accelerographs (triangles) superimposed on a map of the Imperial Valley. The lines trending NNW and north, are the Imperial and Brawley faults, respectively. Cross marks the epicenter. Only the first 10 sec, after triggering, of the particle accelerations are shown.

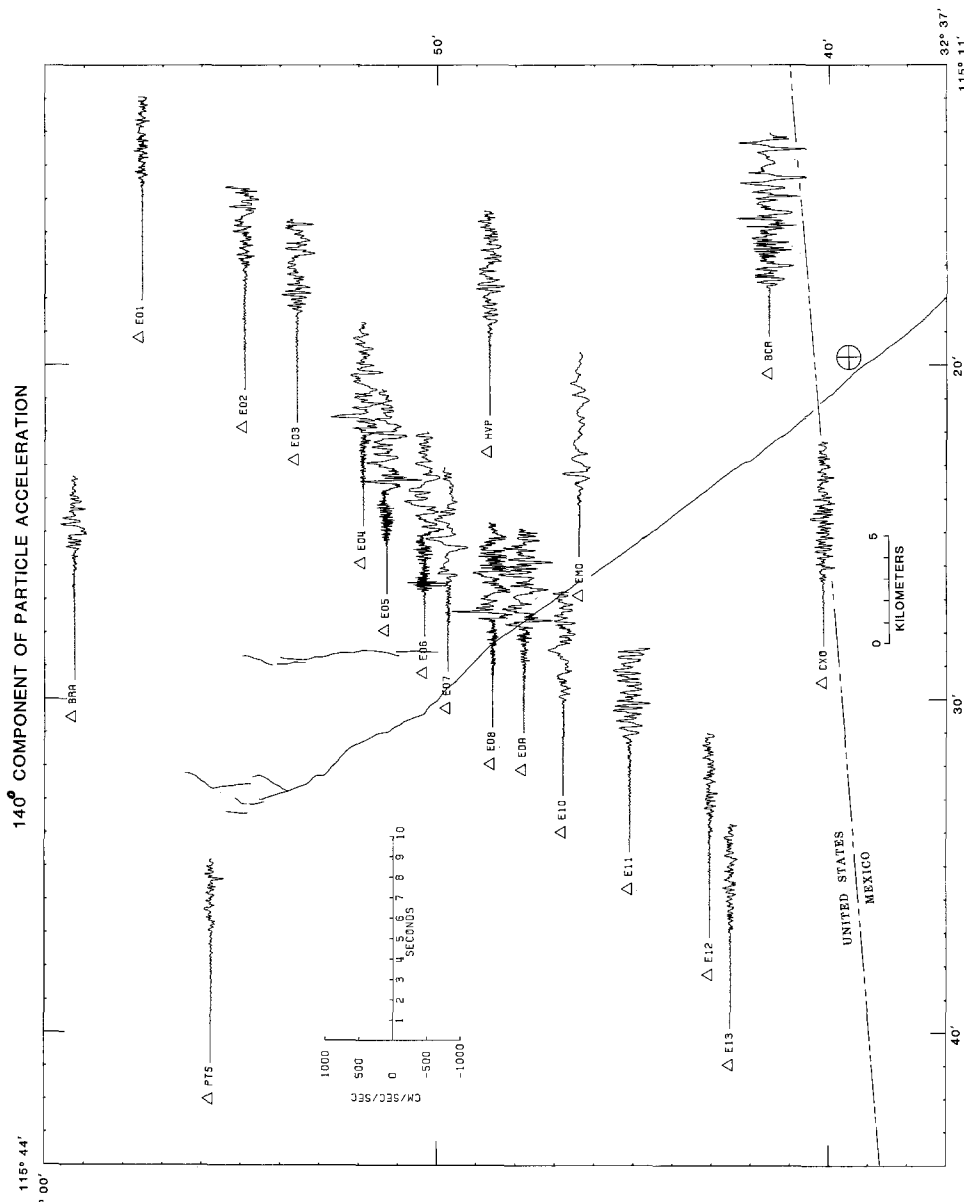


FIG. 5. Main shock 140° component of particle acceleration. See caption of Figure 4 for further explanation.

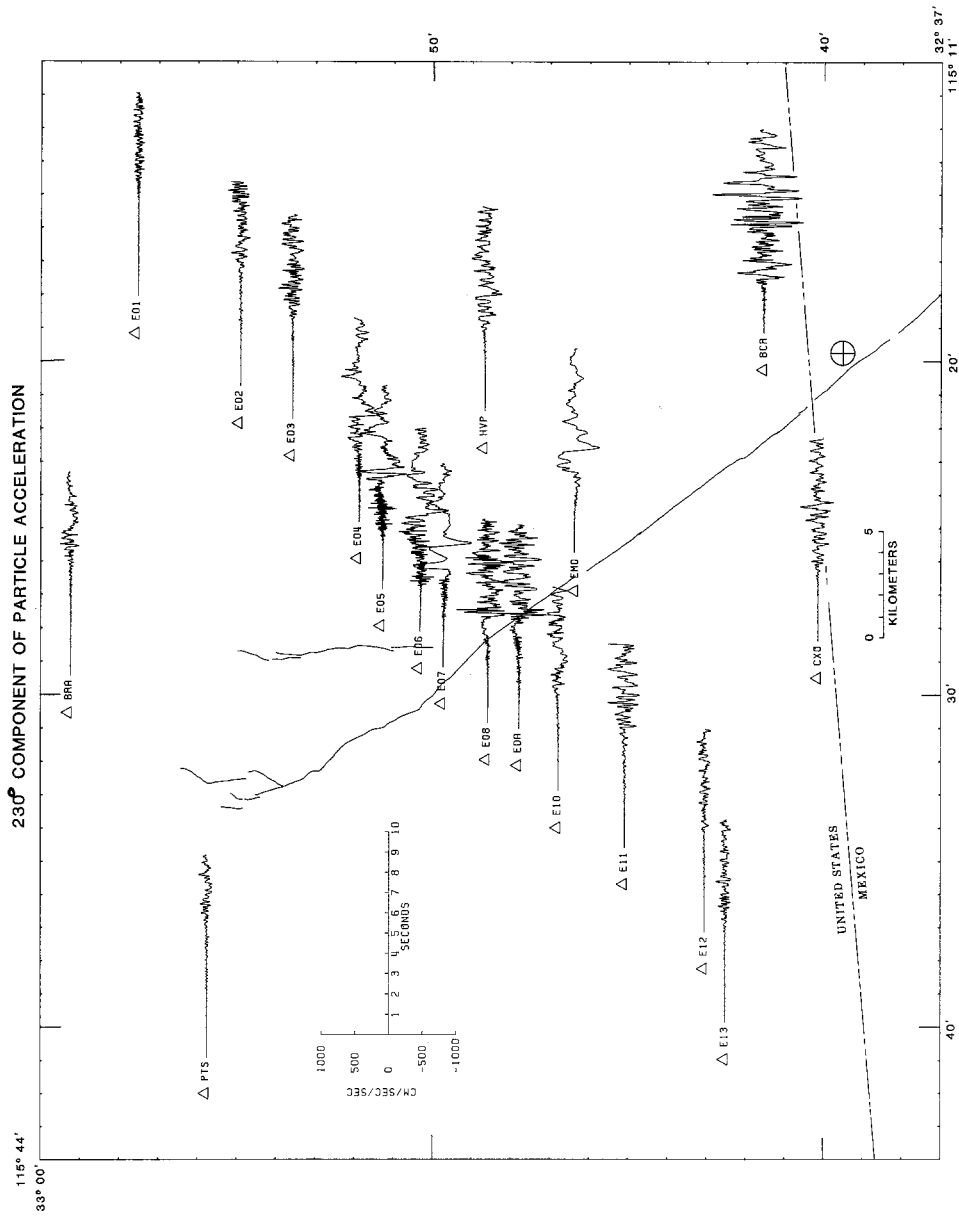


FIG. 6. Main shock 230° component of particle acceleration. See caption of Figure 4 for further explanation.

component of particle velocity dominates, with values of 115 cm/sec at EMO (Meloland) and 108 cm/sec at E06 and E07. Although these values are among the highest particle velocities ever recorded, the feature that stands out in Figure 9 is the remarkable similarity and simplicity of the waveforms. If the faulting were pure strike-slip on a vertical plane in a laterally homogeneous medium, the 230° component would be perfectly symmetrical about the fault plane. It is obvious from Figure

TABLE 1  
SELECTED STRONG MOTION STATIONS IN THE UNITED STATES AND MEXICO

Station	Code	Latitude (N) (deg min)	Longitude (W) (deg min)	Trigger* Time (min:sec)	Epicentral Distance (km)	Azimuth† (deg)
Aeropuerto‡	APO	32 39.00	115 19.80	NAT	0.93	140.0
Bonds Corner	BCR	32 41.56	115 20.25	16:57.11	3.88	-29.6
Islas Agrarias‡	AGR	32 37.25	115 18.07	16:56.88	4.96	173.0
Mexical‡	MEX	32 37.20	115 25.20	NAT	9.45	76.8
Calexico	CXO	32 40.16	115 29.49	16:58.87	15.18	45.4
Meloland§	EMO	32 46.38	115 26.88	16:59.70	16.86	1.0
Holtville	HVP	32 48.71	115 22.59	NAT	17.59	-25.6
Chihuahua‡	CHI	32 29.00	115 14.20	16:59.32	21.31	164.2
Compuertas‡	COM	32 34.80	115 5.40	NAT	24.11	-151.2
Differential Array	EDA	32 47.83	115 32.11	NAT	24.63	11.3
EC Array 6	E06	32 50.36	115 29.20	17:01.40	24.90	-3.9
EC Array 4	E04	32 51.93	115 25.91	17:01.78	24.91	-17.5
EC Array 7	E07	32 49.77	115 30.26	NAT	25.06	0.7
EC Array 5	E05	32 51.33	115 27.93	17:01.39	25.31	-9.9
EC Array 8	E08	32 48.63	115 31.94	17:00.62	25.39	8.3
EC Array 9	E09	32 47.75	115 32.92	NAT	25.54	13.3
EC Array 10	E10	32 46.82	115 33.98	NAT	25.96	18.5
Cerro Prieto‡	CPO	32 25.52	115 18.34	16:58.84	25.97	-145.0
Imperial County Center§	ICC	32 47.57	115 33.81	NAT	26.49	15.7
EC Array 3	E03	32 53.63	115 22.82	NAT	26.58	-29.8
EC Array 11	E11	32 45.12	115 35.68	17:00.48	26.89	27.2
EC Array 2	E02	32 54.96	115 21.85	17:01.18	28.79	-33.6
EC Array 12	E12	32 43.07	115 38.24	17:01.48	29.54	37.1
EC Array 1	E01	32 57.59	115 19.17	17:02.24	33.49	-41.7
EC Array 13	E13	32 42.54	115 40.96	17:02.45	33.51	40.4
Delta‡	DEL	32 21.37	115 11.70	17:01.39	35.86	160.7
Cucapan‡	CUC	32 18.30	115 19.92	NAT	39.23	139.7
Brawley	BRA	32 59.30	115 30.54	17:03.54	40.29	-15.40
Victoria‡	VIC	32 17.40	115 6.00	NAT	46.23	167.8

\*All times are for 23 hour 15 October 1979 UTC. NAT, no absolute time.

† The angles are degrees measured from the strike of the fault N40°W. Positive angles are counter-clockwise; negative angles are clockwise.

‡ Strong motion stations operated jointly by the Instituto de Ingenieria, Universidad Nacional Automa de Mexico and the Institute of Geophysics and Planetary Physics, Scripps Institution of Oceanography, University of California, San Diego.

§ Strong motion stations operated by the California Division of Mines and Geology.

9 that the east side of the fault has larger amplitudes when comparing E05 with E08 and E04 with EDA. For perpendicular distances greater than about 12 km, between a station and the fault, the amplitudes are roughly equal on both sides of the fault. Both the lateral variations in the velocity structure across the Imperial fault and the northeastward dip of the Imperial fault contribute to this asymmetry.

Two aspects of the particle velocities in Figure 9 are due to the nature of a propagating rupture. First, the amplitudes are larger and more pulse-like at the

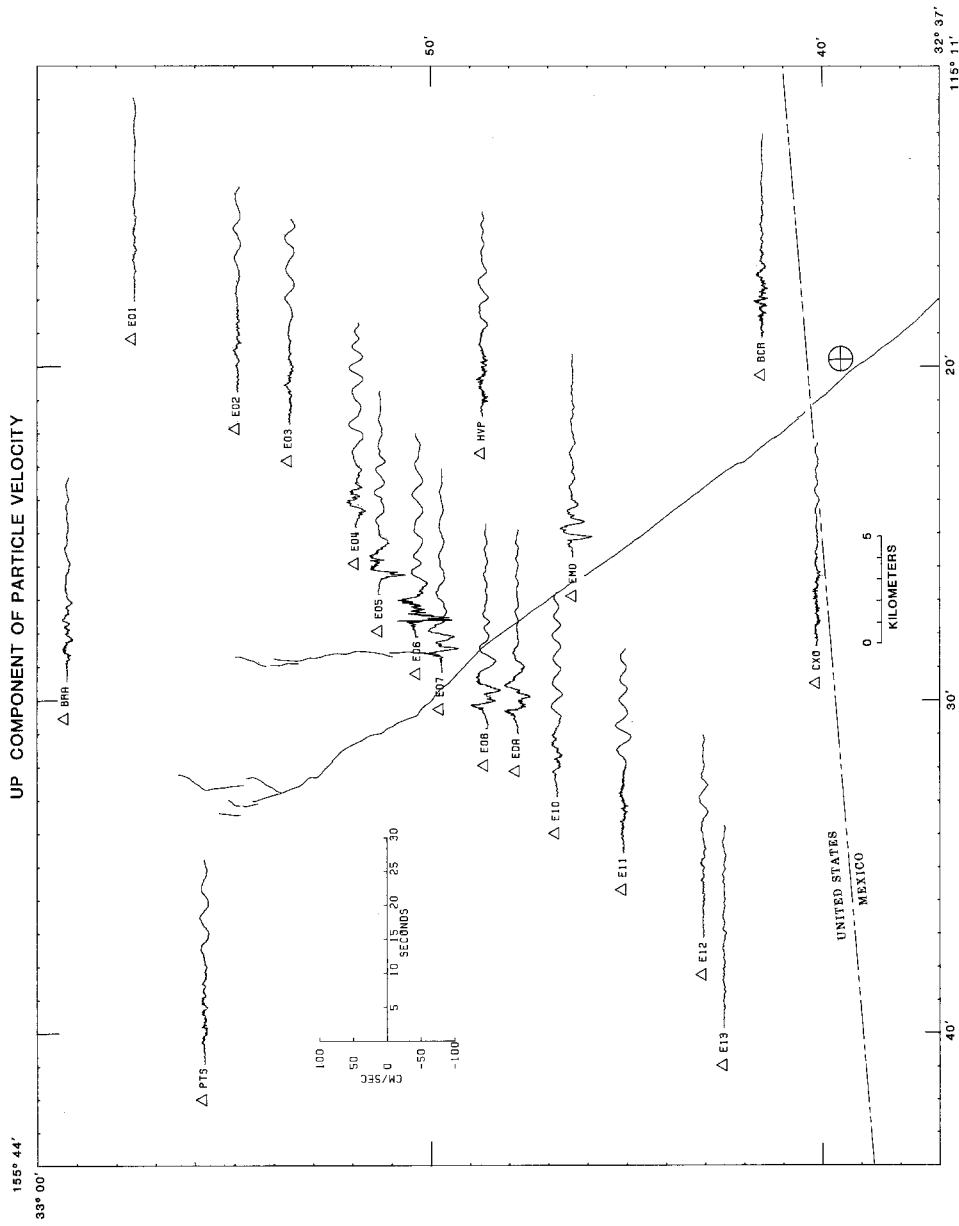
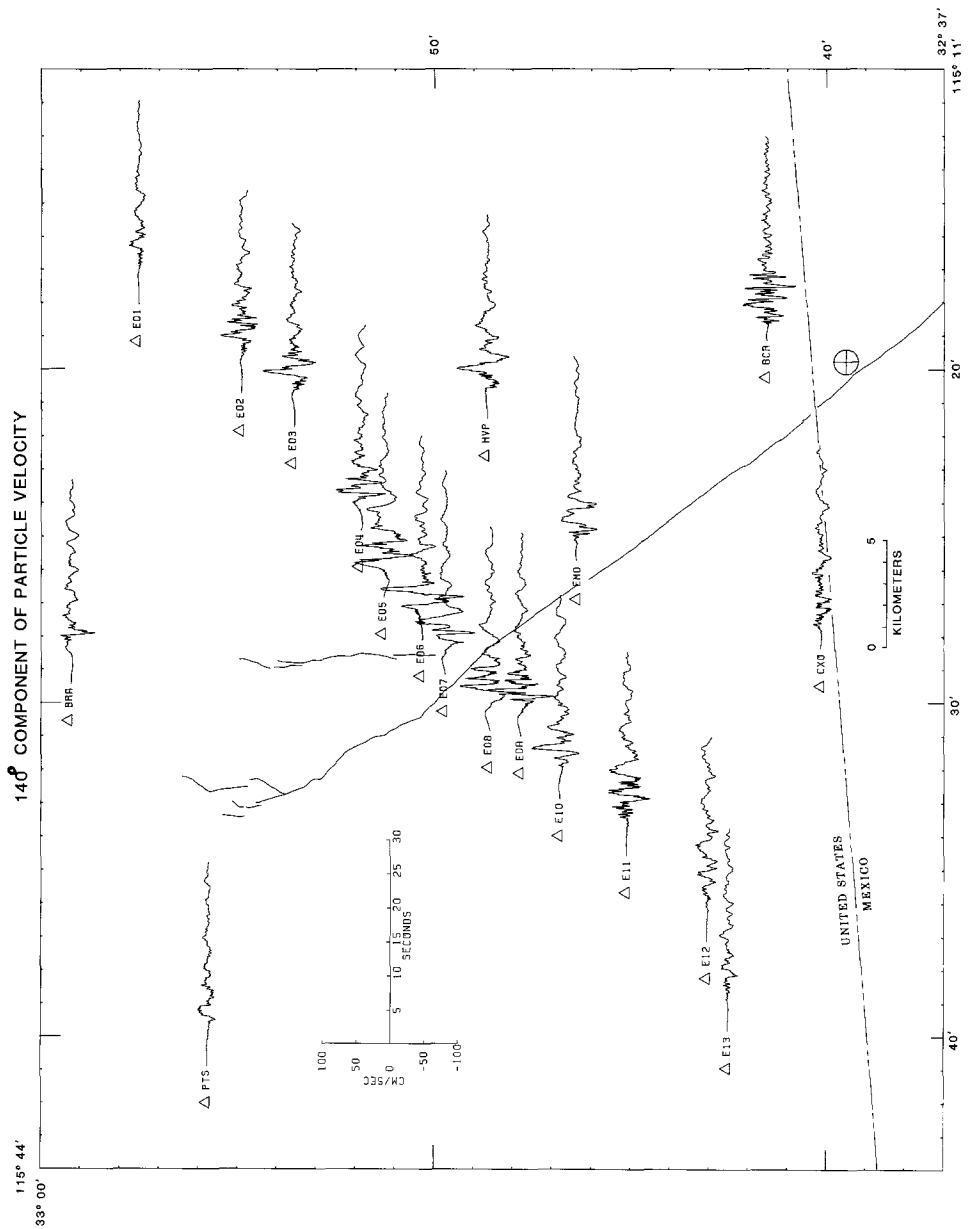


FIG. 7. Main shock vertical component of particle velocity obtained by integrating the vertical particle acceleration. The first 30 sec after triggering is plotted. See caption of Figure 4 for further explanation.



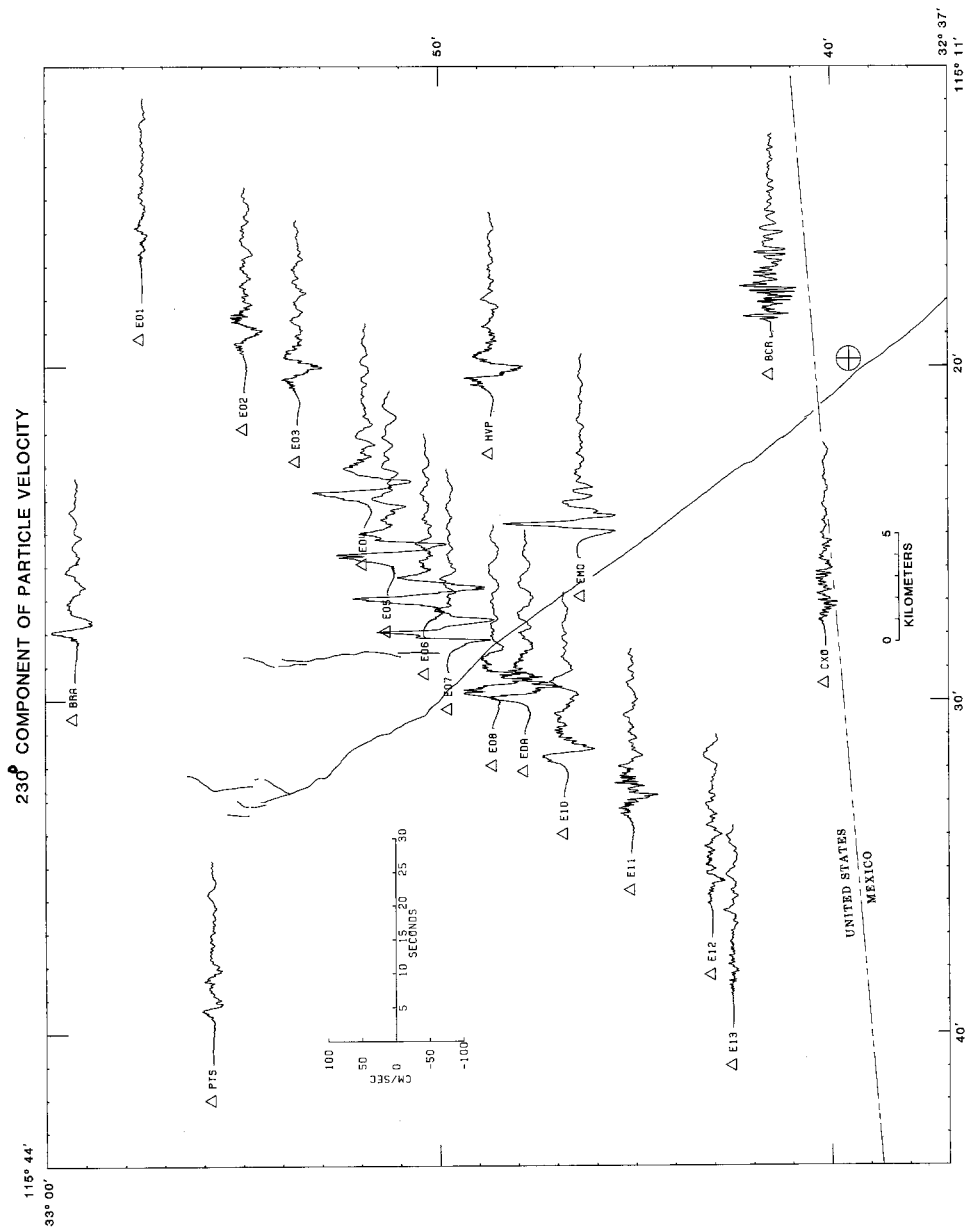


FIG. 9. Main shock  $230^\circ$  component of particle velocity obtained by integrating the  $230^\circ$  component of the particle acceleration. The first 30 sec after triggering is plotted. See caption of Figure 4 for further explanation.

northern stations than at the stations near the epicenter. Second, stations such as HVP, E02, E03, and E11 have pulse shapes similar to one another but different from the pulse shape at E06, for example. The observation that the amplitudes are larger and more pulse-like in the direction of propagation is the effect of focusing from a propagating rupture. Near-source studies of a propagating stress drop in a half-space (Archuleta and Frazier, 1978) and in a vertically varying medium (Archuleta and Day, 1980) show that the near-source particle velocities are amplified in the direction of rupture propagation. This amplification is due not only to directivity (Ben-Menahem, 1962) but also to a feedback mechanism when the rupture velocity is less than the local shear wave velocity (Archuleta and Frazier, 1978). However, if we assume a uniform stress drop moving at a constant rupture velocity, focusing cannot explain the amplitude difference on the 230° component of EMO compared to E06 or E07. EMO is closer to the epicenter than E07. If focusing due to a uniform stress drop moving at a constant velocity were the only cause of larger amplitudes, EMO should have a smaller amplitude than E07 (Archuleta and Frazier, 1978; Archuleta and Day, 1980), but the reverse is true. This suggests that either the stress drop or the rupture velocity is not uniform along the fault strike.

The horizontal particle velocity oriented parallel to the strike of the fault is shown in Figure 8. Note that it has considerably smaller peak amplitudes than the corresponding perpendicular component. The parallel component of motion would be expected to show antisymmetry with respect to a vertical fault in a laterally homogeneous medium. As a consequence, stations near the fault would be nodal. Clearly the 140° component of motion at stations EMO, E06, and E07 is not nodal, just as the vertical motion was not nodal. Since a vertically heterogeneous medium cannot, by itself, influence the position of a nodal plane relative to a vertical fault, the motion on the 140° and vertical components is further evidence of dip on the Imperial fault and lateral heterogeneity across the fault.

#### RUPTURE VELOCITY

As discussed in a later section, the measurements of the static horizontal and vertical slips strongly support the idea that the rupture passed between stations E06 and E07 during the earthquake. Assuming that the dynamic rupture did indeed pass between E06 and E07, one might expect to see some obvious evidence in the seismograms that indicated the time of the passing of the rupture. In particular, one might expect that the motion parallel to the strike of the fault (the 140° component) would become strongly antisymmetric between E06 and E07 at the time of the passing of the rupture (Archuleta and Frazier, 1978). As discussed below, such is not the case. Apparently, the complexities due to the velocity structure, depth of faulting, and the dip of the fault obscure any direct measurement of the time of the passing of the rupture. Thus, one must deduce the probable rupture velocity from physical arguments. Before I do this, I explain what the phrase "passing of the rupture front" means in a vertically varying medium.

Of course, one can only observe waves emitted by the rupture front, not the rupture front itself. In the case of the 140° component for stations E06 and E07 close to the fault, but on opposite sides, one would like to determine the point at which there is strong antisymmetry in the particle acceleration or the slope of the particle velocity between the two stations due to their being at maxima in opposing polarity lobes of the rupture's *SH* radiation pattern as the rupture passes. In the case of the 230° component, which is nearly symmetric for stations E06 and E07, one would first wish to determine the time when the observed waves change from

originating from the leading lobe of the moving double-couple's radiation pattern to originating from the following lobe. Since the shear-wave velocity in the basement (between depths of 5 and 10 km) of the Imperial Valley is so much greater than that at the surface (Figure 2), it is likely that the rupture at depth will pass beneath stations E06 and E07 much earlier than the surficial rupture. If most of the seismic energy is liberated in the basement, then the observed polarity changes will most likely be related to the passage of the rupture at depth.

The most direct measurement of the arrival of the rupture front might have come from examination of the  $140^\circ$  component of particle velocity or acceleration at stations E06 and E07. Once the rupture had started to pass between the two stations, which are on opposite sides of the fault, the particle motion would clearly be  $180^\circ$  out of phase. Unfortunately, station E07 does not have absolute time, so it is not clear where we should look for this  $180^\circ$  phase difference in the particle motion. I have attempted to assign timing to E07 relative to E06 by cross correlating its  $230^\circ$  particle velocity with the  $230^\circ$  particle velocity at station E06. The  $230^\circ$  component can be used because this motion is continuous across the fault and because both E06 and E07 are in almost the same place relative to the radiation coefficient for this component of motion. Even if absolute time were available on E07, this would be the appropriate procedure to follow since it removes the effects of near-surface delays. From this cross correlation, I determined that the time series from station E07 should be shifted 0.3 sec earlier to align with E06. However, there is evidence from an aftershock study (Boore and Fletcher, 1982) that S waves arrive about 0.5 sec later at E06 than at E07 for earthquakes south of those two stations. Combining these two results to assign absolute time to E07, I infer that E07 triggered 0.8 sec before E06.

In Figure 10 is shown the first 16 sec of the three components of particle velocity for stations E06 and E07, with the time series for E07 shifted by 0.3 sec relative to E06 based on the cross correlation only. In Figure 10, the positive motion for the particle velocity is in the up,  $230^\circ$ , and  $140^\circ$  directions. A primary consideration in examining the  $140^\circ$  components is that the acceleration should be in the  $320^\circ$  direction at E07 and in the  $140^\circ$  direction at E06 for a right-lateral vertical fault rupture that passes between them. After the arrival of the first S waves from the hypocenter, there are two places where the  $140^\circ$  components of velocity on E06 and E07 have opposite slopes. These two places are indicated by the vertical dashed lines in Figure 10. The earlier time is 5.8 sec after trigger time on station E06 and the later time is 6.3 sec after trigger time. If one adds these numbers to E06 trigger time, one finds that the S waves from the rupture arrived either 12.8 or 13.3 sec after origin.

The second method of inferring the time of arrival of S waves from the rupture front is by studying the polarization of the particle velocity for stations near the fault. The initial direction of polarization due to the near-field terms should be opposite to that of the S-wave field; hence, the initial particle velocity will be in the  $50^\circ$  direction. When the S waves from the hypocenter arrives, the particle velocity will move in the  $230^\circ$  direction. Once the rupture passes the observation point, the particle velocity will start to move in the  $50^\circ$  direction because the sign of the lobe of the S-wave radiation changes sign. To illustrate these main points, I show in Figure 11 a polarization diagram for the motion at station E06.

The  $140^\circ$  component of particle velocity is shown along the abscissa; the  $230^\circ$  component is shown along the ordinate. On the  $45^\circ$  line, the polarization is plotted as a function of time. The time axis on the  $45^\circ$  line is stretched by the factor  $\sqrt{2}$ .

relative to the orthogonal axes. For each tenth of a second, the magnitude of the polarization  $P = \sqrt{\dot{u}(140)^2 + \dot{u}(230)^2}$  and the angle of polarization  $\theta = \arctan(\dot{u}(230)/\dot{u}(140))$  is computed. The length of each ray on the  $45^\circ$  axis is  $P$ ; the angle is  $\theta$ . I have drawn a circle of radius 100 cm/sec and labeled the primary angles for interpretation of the magnitude and direction of the polarization.

Initially, the particle motion is almost entirely polarized in the  $50^\circ$  azimuth, consistent with the near-field term for this station and a right-lateral strike-slip fault. With the arrival of the S waves, the polarization reverses direction to the  $230^\circ$  azimuth. About 6.0 sec after trigger, the polarization starts to rotate toward the  $320^\circ$  direction; at 6.3 sec it is parallel the  $320^\circ$  direction, and shortly thereafter reverses

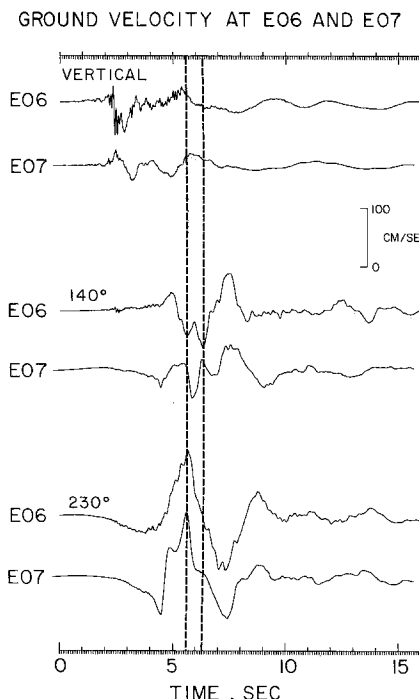


FIG. 10. Comparison of the first 16 sec of the three components of particle velocity at stations E06 and E07. Station E07 has been shifted 0.3 sec relative to E06 based on a cross correlation of E06 and E07. Two choices for the time of rupture front passing at depth between the two stations are shown by vertical dashed lines. See Figure 4 for station locations.

to the  $50^\circ$  azimuth. A similar polarization diagram can be constructed for station E07, although the reversal from  $230^\circ$  to  $50^\circ$  occurs about 0.3 sec later than it does at station E06. The polarization results corroborate the earlier result that the change observed on the  $140^\circ$  components is due to S waves from the rupture front passing these two stations. However, the polarization diagram does not necessarily indicate which of the two points in time is preferable.

Because of the tradeoff between the source time function and the rupture velocity (Anderson and Richards, 1975), one might suspect that a very short source time function is responsible for the reversal in the polarization diagram, i.e., the change in the particle velocity from the  $230^\circ$  direction to the  $50^\circ$  direction. However, I have calculated synthetic seismograms that indicate that varying rise times do not significantly affect the rupture velocity determination. To illustrate this point, I

show in Figure 12 synthetic particle velocities for the  $230^\circ$  component computed from a fault 35 km long and 10 km deep dipping  $75^\circ$  in a laterally homogeneous medium with a vertical velocity profile given by Figure 2, except that I used a surficial shear velocity of 0.8 km/sec to reduce computational costs. The synthetic seismograms were calculated using the method of Spudich (1981) and the discrete-wavenumber finite-element method of Olson (1982). The receiver is in the same location relative to the fault and hypocenter as E06 is to the Imperial fault. Since I am only interested, at this time, in demonstrating how the particle velocity is

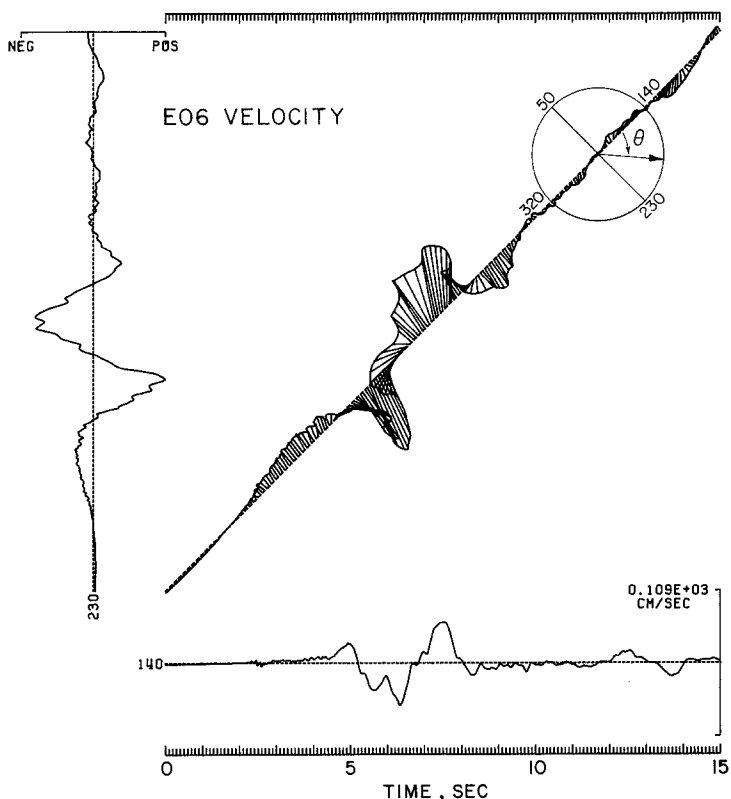


FIG. 11. Polarization plot constructed from the two horizontal components of particle velocity at station E06. Ordinate is  $230^\circ$  component; abscissa is  $140^\circ$  component. Along the  $45^\circ$  line, polarization magnitude and direction are plotted as a function of time. See text for definition of polarization magnitude and angle. Circle with amplitude 100 cm/sec and four principal angles show direction and scale of the polarization.

affected by either the rupture velocity or the duration of the slip function, I assume that the slip velocity function is a rectangle with an amplitude variation over the fault that remains the same for each computation. The duration of the rectangle is constant for each computation as indicated on Figure 12. Since the duration is allowed to vary for the different computations but the amplitude stays constant, the seismic moment also varies. It is this variation that leads to the different amplitudes, which are irrelevant in this discussion. In four of the synthetics, the duration is fixed at the same value, but the rupture velocity is a different constant fraction of the local shear wave velocity. In three of the synthetics, the rupture velocity is a constant fraction of the local shear wave velocity but the duration of the slip velocity is different. The time at which  $S$  waves from the rupture at depth reach the station

is indicated by a dot on each synthetic seismogram. It is clear in these examples that the time at which the rupture passes the station at depth is at or after the peak in the particle velocity on the  $230^\circ$  component.

From the preceding analysis, it appears that  $S$  waves emitted from the rupture front as it passed between E06 and E07 arrived at E06 and E07 12.8 to 13.3 sec after the origin time. These values lead to rupture velocity estimates in the basement of 2.6 and 2.5 km/sec, respectively, or about 0.78 times the local basement shear velocity on the east side of the fault. These values are easily calculated from the 24.9 km epicentral distance to E06, an average basement shear velocity of 3.2 km/sec, and a 3.2 sec delay for shear waves generated at 5 km depth to travel vertically to the surface using the assumed  $S$ -wave velocity structure in Figure 2.

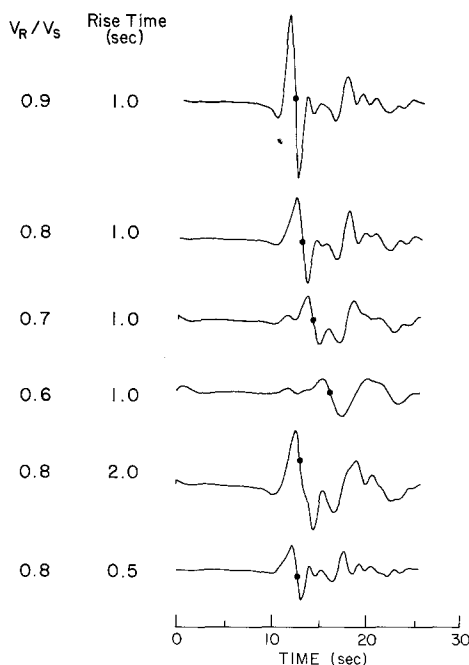


FIG. 12. Synthetic particle velocities from extended sources. Either the ratio of rupture velocity to local shear velocity or the duration of the rectangle time function for the slip velocity varies between traces. The component of motion is equivalent to the  $230^\circ$  component for station E06 relative to the Imperial fault. Dot shows the theoretical time at which rupture at depth is passing the station.

If the rupture velocity is a known fixed fraction of the shear velocity at all points along the rupture, then it is easy to estimate the rupture evolution since the paths of "rupture rays" (points on the rupture front moving normally to it) are governed by Snell's law and follow exactly the same paths  $S$  waves would follow. Using the estimate of 0.78  $V_s$  and a two-dimensional ray-tracing program (Červený *et al.*, 1977), the evolution of faulting north of the hypocenter is shown in Figure 13. A cross section of the Imperial Valley in the plane of the fault is shown at the *bottom*. On the fault, the position of the rupture front is indicated at 2-sec intervals after origin time. The dashed lines represent the fact that the exact depth of faulting is unknown and the rupture did not break the surface for 7.5 km north of the hypocenter. In the *upper panel*, the approximate time at which the rupture breaks

the surface is plotted against distance along the fault. This time is slightly earlier than the true value because I could not incorporate the steep S-wave velocity gradient in the upper 0.35 km into the ray-tracing program. I simply extrapolated the S-wave velocity profile below 0.35 km to the surface, thereby overestimating the surficial S-wave velocity and giving a faster velocity to our rupture front in the upper 0.35 km.

#### LARGE AMPLITUDE VERTICAL ACCELERATIONS (LAVAs)

One of the most interesting features of the near-source ground motion is the presence of the LAVAs at some, but not all, of the recording sites. As discussed earlier, the maximum acceleration of 1705 cm/sec<sup>2</sup> at station E06 is due in part to a local amplification by a factor of 3 (Mueller and Boore, 1981). Nevertheless, stations E05, E06, E07, E08, and EDA (Figure 4) and five digital strong motion stations, the differential array (Bycroft, 1980), within 225 m of EDA all show peak vertical acceleration larger than or comparable to either component of horizontal

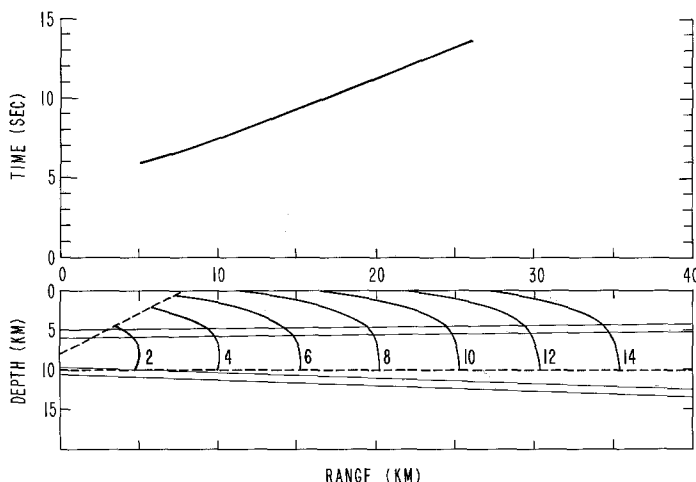


FIG. 13. Position of the rupture front on a cross section of the Imperial fault shown at 2-sec intervals after initiation assuming rupture propagation with a velocity of 0.78 times the local shear wave velocity. Travel-time curve (top) gives the time at which the rupture front breaks the earth's surface.

acceleration. The same type of phase, reduced in amplitude, is observed at E04 and HVP. LAVAs have four important characteristics: (1) they were recorded on stations all at about the same epicentral distance; (2) at each of these stations the LAVA arrived before the S wave from the hypocenter; (3) LAVAs are all clearly observed within 11 km on either side of the fault trace; and (4) relative to the fault strike, they are near the P-wave node in the radiation pattern.

What caused this phase? Is it primarily due to the earthquake rupture or is it due to a propagation effect? Since this phase arrives before the S wave from the hypocenter, it must travel part of its path as a P wave, presuming subshear rupture velocity. This conclusion is supported by the fact that the amplitude is much larger on the vertical component than on either horizontal. If we use the result of the preceding section, i.e., that the average rupture velocity is less than the local shear wave velocity, then travel-time considerations eliminate the possibility that this phase is a P wave which was converted from an S wave at the free surface. Such a phase will always arrive after the LAVAs for the following reason. Since in Figure 3b it can be seen that sP always arrives earlier than SP at equal epicentral range,

one needs to consider only  $sP$ . Assume momentarily that the rupture velocity equals the local shear velocity. Then rupture ray paths and travel times are identical to  $S$  ray paths and travel times. By Fermat's principle, the path of  $sP$  from the hypocenter to the observer is a minimum time path, and consequently its arrival time is also the earliest possible for an  $sP$  generated anywhere on the fault. Since the stations observing the LAVAs are at about 25 km epicentral range, Figure 3b shows that the earliest possible  $sP$  arrival time is 10.4 sec after origin, which is about 1 sec after the LAVAs are actually observed. This time discrepancy becomes even greater if the rupture travels at less than the local shear velocity.

While one can rule out  $S$  to  $P$  conversion at the free surface by timing arguments, one cannot exclude the possibility of an  $S$  to  $P$  conversion at an internal boundary using timing. However, fairly substantial velocity discontinuities are necessary to generate such converted phases, and no such discontinuity has yet been detected in the central Imperial Valley (Fuis *et al.*, 1982). Since any  $S$  to  $P$  conversion is unlikely, one is limited to phases that travel their whole path as compressional waves, direct  $P$  or  $PP$ . Any other  $P$  phase will have travel times that are too late to match the observed times of arrival.

Since the LAVAs are probably  $P$  or  $PP$ , it is curious that they are so large near the fault trace which is a node for  $P$ -wave radiation from a vertical strike-slip or dip-slip fault in a laterally homogeneous medium. Two effects occur in the Imperial Valley which may partially diminish the nodal character of the fault trace. First, the refraction work of Fuis *et al.* (1982), particularly the 6NW-1SE profile, shows a change in the velocity structure across the Imperial fault, the west side of the fault having  $P$  velocities at most 0.5 km/sec faster than the east side. While this leads to the possibility of lateral refraction of  $P$  waves back onto the fault trace, it would be surprising if this rather small lateral change were sufficient to generate the LAVAs near the fault trace. A second factor that would diminish the nodality of the fault trace is the likelihood that the Imperial fault dips about 75°NE. A dip would diminish the nodal character of the fault trace since a  $P$ -wave initially emitted traveling parallel to the fault surface (a nodal  $P$  wave) would be refracted upward and out of the fault plane, emerging at the earth's surface shifted off the surface fault trace. The amount of shift would vary depending on the source depth and epicentral range of the  $P$  wave. For example, if one uses the  $P$ -wave velocity profile for the Imperial Valley for a strike-slip point source buried 4 km deep on a fault that dips 77°, the nodal  $P$  observed at 18 km epicentral range will be shifted 4 km off the fault trace onto the hanging side of the fault; for the same source, nodal  $PP$  will emerge about 0.25 km off the trace in the same direction.

While these two factors may operate to smear out the  $P$ -wave node near the fault trace, a glance at Figure 4 shows the LAVAs to be distinctly antinodal in character near the fault trace. Hence, I must conclude that one cannot always expect to observe  $P$ -wave nodes where they are theoretically predicted in this region.

Ironically, while the LAVAs are dominant near the fault trace where one would expect a nodal character, they become very small off the fault where one would expect amplitude maxima. In particular, I note in Figure 4 that they are large at EDA and nonexistent at E10, only 3 km farther west, and at all other stations west of E10. Similarly, on the east side of the fault, the LAVAs are diminishing at E04 and nonexistent for stations to the east of E04. This observation places a strong constraint on their source and propagation paths. Having already deduced that the LAVAs are either a direct  $P$ - or  $PP$ -type phase, let us consider the consequences of these two possibilities.

First let us assume that the LAVAs are direct  $P$  waves. Except for the influence

of theoretical radiation pattern nodes, there is no known factor that would prevent  $P$  waves emitted from any point on the Imperial fault from being observed throughout the Imperial Valley. Although I have discounted the usefulness of radiation pattern nodes for explaining the existence of LAVAs near the fault, one must invoke radiation pattern nodes to explain the nonexistence of LAVAs at E10 and west and east of E04 if they are direct  $P$  waves. The high-frequency content and the duration of 1 to 1.5 sec imply that the LAVAs were generated on a small part of the fault. The least exotic possibility is that they were generated when a small region of the fault broke with a large stress drop and subshear rupture velocity. In this case, the  $P$ -wave radiation pattern would be nearly the usual four-lobed double-couple radiation pattern with a very slight modification for  $P$ -wave directivity. Depending on the precise nature of this source, it is unlikely that a small source region can have radiation pattern nodes at all stations east of E04, at E10 and all stations to the west of it, and at BCR and CXO, although I have not done a feasibility study of such a source. Another consequence of this source is that at regional distances,  $P$  waves from the hypocenter would travel nearly identical paths to regional observers as  $P$  waves from the high-stress drop region. Hence, a large stress change occurring after the rupture began should cause a sudden amplitude change in the  $P$ -wave train of seismograms recorded at regional distances. With this in mind, I examined the records of 14 U.S. Geological Survey low-gain, three-component seismometers in central and northern California (epicentral distances on the order of 600 to 1200 km), but other than changes associated with  $P$ -wave crustal and Moho phases, I found no amplitude changes larger than a factor of 2.

Hartzell and Helmberger (1982) identified the LAVAs with direct  $P$  waves from a region of large (200 bars) stress drop. To satisfy timing requirements, they place this region at 8 km depth under station EMO. A difficulty with this hypothesis, which they recognized, is that stations E10 and E04 lie almost exactly on a  $P$ -wave radiation pattern maxima for a strike-slip source beneath EMO. To explain the absence of LAVAs at these and more distant local stations under the direct  $P$  hypothesis, it becomes necessary to invoke a source having appropriately placed radiation pattern nodes.

The theoretical  $P$ -wave radiation pattern can be altered from the usual double-couple radiation pattern by a sudden change in the rupture velocity, or by a rupture propagating near the  $P$ -wave velocity. The least likely of these two possibilities is that the LAVAs are produced by a rupture deceleration from near the shear velocity to zero, or acceleration from zero to near shear velocity. Both Madariaga (1977) and Boatwright (1982) showed that in these situations,  $P$ -wave radiation is slightly enhanced in the backward direction, which completely contradicts the observations. [I presume here that if the LAVAs are direct  $P$  waves, their source is southeast of E06 and E07, consistent with the timing arguments of Hartzell and Helmberger (1982).] The second possibility is that at some point south of E06, the rupture accelerated from subshear to nearly  $P$ -wave velocity. Very little theoretical work has been done on acceleration pulses radiated in this situation, but it is likely that  $P$  waves would be focused in the forward direction. Theoretically, once accelerated to near  $P$  velocities, the normal directivity (Ben-Menahem, 1962) for  $P$  waves would continue to focus energy in the forward direction.

It is difficult to say whether the available data support the possibility of supershear rupture velocity occurring for more than 1 sec or so. By inverting observed accelerations in the period range of 3 to 10 sec, Olson and Apsel (1982) have obtained results which could be interpreted as supporting a 4.5 km/sec rupture velocity over

a 20-km portion of the Imperial fault beneath 5 km depth. They caution that this velocity is a horizontal phase velocity, and the true velocity may be lower depending on the vertical component of the rupture velocity. Hartzell and Helmberger (1982) used a 2.5 to 2.7 km/sec rupture velocity to model the observed displacements, although they speculated that the LAVAs resulted from the supershear rupture of a localized asperity beneath EMO. Niazi (1982) obtained a 2.7 km/sec rupture velocity estimate by examining *P*-wave particle motions; preliminary results of Spudich and Cranswick (1982) also indicate a 2.5 km/sec rupture velocity up to and possibly during the time of generation of the LAVAs. While not supporting a supershear rupture velocity, their preliminary work supports the proposal that the LAVAs are direct *P* waves originating from an area about 17 km north of the hypocenter. This region of the fault is about 3 km south of the area that has the maximum displacement in the model of Hartzell and Helmberger (1982).

Thus, some evidence supports the hypothesis that the LAVAs are direct *P* waves, although to explain their spatially limited range of observation one must invoke a mechanism that uses radiation pattern nodes to account for their small amplitude at HVP, and their nonexistence at all stations west of EDA, east of E04, and at EMO, the station closest to their presumed origin. In view of the lack of any observable *P*-wave node near the fault trace, the fortuitous combination of a node and a significant site effect would probably be required to explain the abrupt disappearance of the LAVA between EDA and E10. Any mechanism requiring sustained rupture propagation at supershear velocities is not unambiguously supported by the strong motion data.

An alternative possibility that explains the limited range of occurrence of the LAVA without recourse to radiation patterns is that the large accelerations result from a phase of the *PP* type generated when rupture breaks into the sediments. A built-in feature of such phases is that their amplitude-distance curves have sharp maxima, which provides a mechanism for focusing energy without invoking source complexity. The *PP* and *PPP* families were prominent arrivals on the vertical seismograms recorded during the refraction survey in the Imperial Valley (McMechan and Mooney, 1980; Fuis *et al.*, 1982). In Figure 14 is a record section of the vertical accelerograms that have absolute time. The travel-time curve of the *PP* phase has taken into account the time necessary for the rupture to propagate from the hypocenter into the sediments using the evolution depicted in Figure 13. The density of the X's is a good indicator of the amplitude. In the lower part of Figure 14, the paths of the geometrical rays that form the *PP* travel-time curve are shown. Note that the source of the *PP* phase is at a depth of 4 and 5.5 km north of the hypocenter. A subset of the *P* waves generated by a stress drop in the sediments reflects off the earth's surface. Because of the large gradient, these waves turn in the sediments, forming a caustic that manifests itself as large amplitude compressional motion over a very limited horizontal range. The strength of the *PP* phase and the short epicentral range at which it is observed directly result from the high gradient of the *P*-wave velocity in the sediments. The large amplitude, compared to direct *P* waves, is due to structure and not to a large stress drop.

Although the travel time is consistent with the data and our faulting scenario, and the flux of geometrical rays indicate large amplitudes, I have also used the method of Kind (1978) to construct synthetic vertical accelerograms from a point double-couple source with 75° dip located at 4 km depth in a velocity structure approximating the Imperial Valley structure (Figure 15). In this velocity structure, the *P* wave *Q* rises linearly from 206 at the surface to 400 at and below 5 km depth.

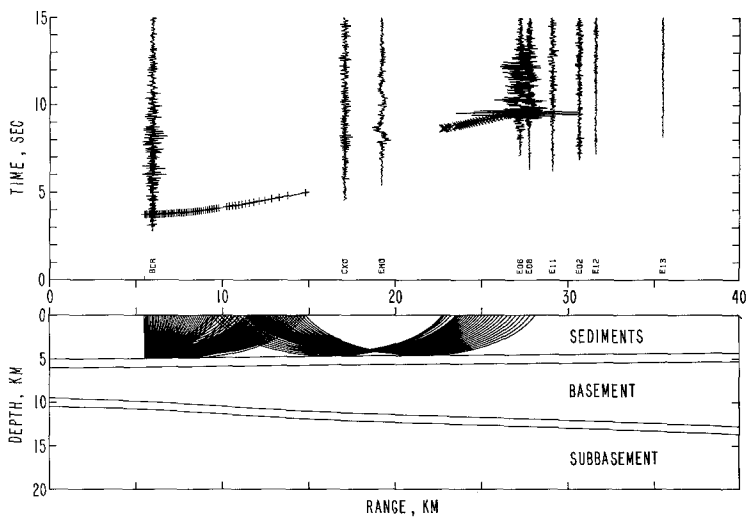


FIG. 14. Record section using vertical accelerations with absolute time shows the travel-time curve for a  $PP$  phase (the line connecting the X's) from a source 4 km deep and 5.5 km north of the hypocenter. Travel-time curve of direct  $P$  from the hypocenter is shown as the dashed line. The lower half of the figure is a cross section of the Imperial Valley showing the geometrical ray paths traveled by the  $PP$  phase.

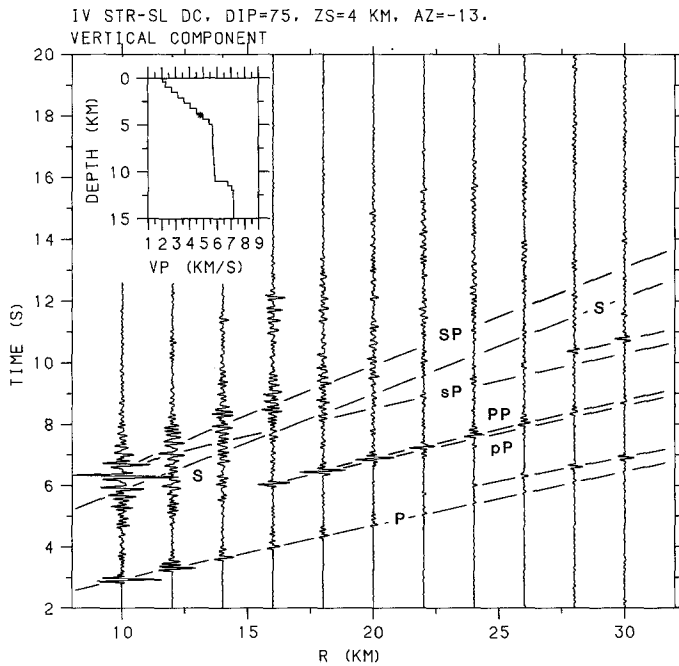


FIG. 15. Record section of synthetic vertical accelerations for a double-couple source with  $75^\circ$  dip at 4 km depth. All ranges are at an azimuth  $13^\circ$  counterclockwise off strike of the double couple. Synthetic accelerograms are computed for the frequency range 0 to 12 Hz. Inset shows  $P$ -wave velocity structure used.

The  $S$  wave  $Q$  was derived from the assumption that all attenuation arose from shear, leading to an  $S$  wave  $Q$  that rose from 34 at the surface to 170 at and below 5 km depth. The ranges are all at an azimuth  $13^\circ$  counterclockwise off strike. Although there are many large amplitude phases present, mostly due to  $SP$  phases, the phase of interest is clearly seen at the ranges of 16 to 22 km. About 2 sec after

the direct  $P$  wave is a large, simple, clean pulse that arrives before the direct  $S$  wave. This pulse is  $PP$ . Note its sudden growth in amplitude at 16 km epicentral range and its limited range of occurrence. It is these attributes that make it a candidate for the LAVAs. Because  $S$  wave  $Q$  is so much lower than  $P$  wave  $Q$ ,  $SS$  phases are not seen in the synthetics.

To see how  $PP$  fits naturally into the picture, consider the following. The large vertical accelerations show up on only a few stations, but all with nearly the same hypocentral distance. The phase arrives after the first  $P$  waves but before the direct hypocentral  $S$  wave. Its amplitude is an order of magnitude greater than the first  $P$  phase, depending on azimuth. Now consider the following scenario for faulting, based on Figures 13 and 14. The rupture nucleates at a depth of 8 km, a depth below the sediments. Since the rupture breaks the surface about 7.5 km north of the epicenter, it obviously propagates into the sediments some time after initiation. After the rupture penetrates the sediments,  $PP$  phases are generated. As the rupture propagates toward the surface,  $PP$  phases from all depths are possible, but the caustic is more diffuse for sources at shallower depths. Once the rupture in the sediments is closer than about 16 km to any station, the  $PP$  phase will cease being observed.

Although the hypothesis that the  $PP$  phase is responsible for the large vertical accelerations reconciles most of the observations with theory, there are some conflicts for which I can offer only *ad hoc* explanations. Namely, once the rupture continues to propagate northward, stations such as E02 or E12 might be expected to fall into the critical range. Why then is there no obvious  $PP$  phase?

One possibility arises from the observation that the strength of the  $PP$  phase depends critically on the velocity structure not only at the source but also at its turning points. Since the sediments in the Imperial Valley thin to the east and west of the fault (Fuis *et al.*, 1982), it is possible that the  $P$  waves reflected from the surface do not turn in the sediments for the stations more than 10 km off the fault. In short, if the sedimentary velocity structure is the same everywhere but the sediments thin as one moves away from the fault, then the turning points, which are necessarily at depths greater than or equal to the source, will not lie in the high gradient zone, and the  $PP$  phase will thus be very weak.

I have examined this possibility. Using a velocity structure in which the sediments thin from 5 to 2 km over a distance of 40 km, a thinning consistent with the results of Fuis *et al.* (1982), I have used the ray-tracing program to look at the dependence of the  $PP$  phase on such a velocity structure. In this shoaling structure, the source, the location where the slip takes place, must be shallower than 4 km to produce a  $PP$  phase with turning points in the sediments. The presence of a dipping sedimentary layer reduces the range over which the  $PP$  phase exists from the 16 to 20 km range to a 14 to 16 km range, with the most intense  $PP$  amplitudes at the closer distance. Using the median range of 15 km, stations E01, E02, E12, and E13 are entirely eliminated from recording  $PP$ . Stations E03, E11, BCR, and CXO would be candidates only after the rupture was farther north than Meloland (EMO). EMO is always at a distance less than the range where  $PP$  can be observed. The vertical accelerogram at HVP shows an abrupt amplitude change that precedes the arrival of the  $S$  wave from the hypocenter. HVP is at an epicentral distance where the geometric rays for  $PP$  will arrive but for a short time, because as the rupture moves north, HVP will move out of the critical range. Because HVP is within the critical range for only a short period of time, the amplitude change on HVP might be expected to be less than that observed on other stations. The only two stations that might be expected to record a strong  $PP$ , but do not, are E04 and E10. The vertical

accelerogram at E04 does show some high amplitudes preceding the arrival time of the *S* wave, although the amplitudes are not as pronounced as at E05. The accelerogram at E10, though, is totally devoid of any amplitudes comparable to those recorded at EDA. The sediments are thinning as one moves in the direction of E04 and E10, but probably not enough to eliminate totally the expected *PP* phase. I am left to speculate that there is some unknown path effect that has eliminated the *PP* phase. This path effect could be subtle and local, since the region on the fault that can generate an observable *PP* phase at E10 and E04 is only about 2 km long. Once the rupture has passed through that region, stations E10 and E04 will be too close to the fault to record *PP*. Another factor that may be contributing

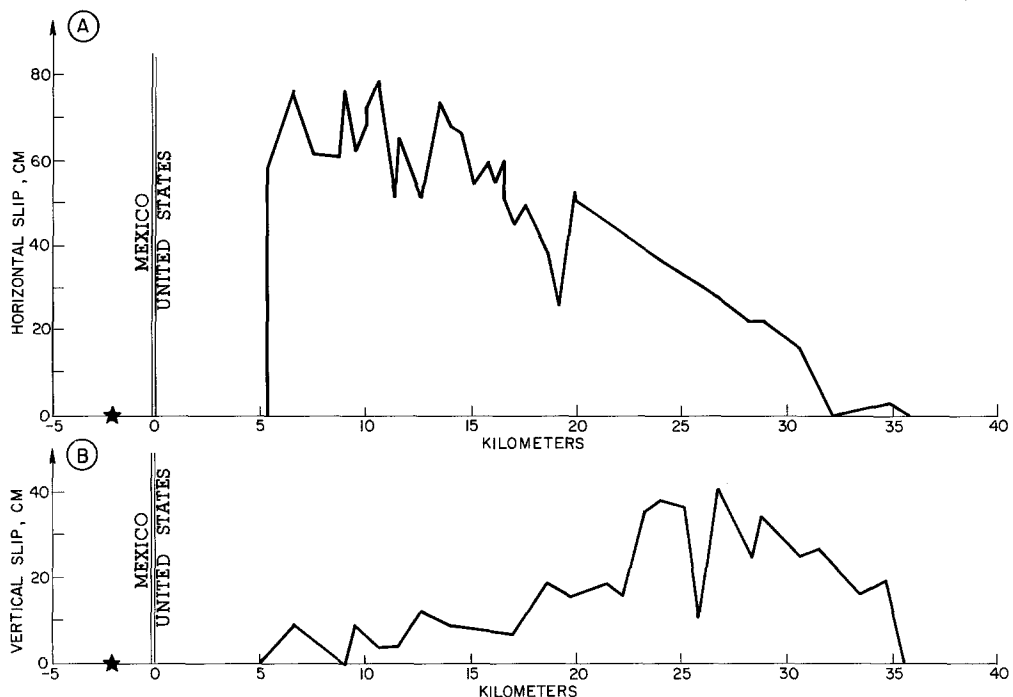


FIG. 16. Surface slip measured about 160 days after the main shock (star = epicenter) plotted against distance along the Imperial fault. (A) Right-lateral horizontal slip. (B) Vertical slip.

to the nonobservance of the *PP* phase is the amount of slip that is occurring in the sediments. If the distribution of surface slip mirrors the amount of slip occurring within the sediments, then the southern part of the fault will be the biggest contributor to the *PP* phase (Figure 16A). The combination of the thinning of the sediments east and west of the Imperial fault and the distribution of slip along the strike of the fault provides a reasonable explanation for why the *PP* phase might or might not be recorded.

#### STATIC MEASUREMENTS

Within 24 hr of the main shock, measurements of right-lateral horizontal offsets and vertical offsets on the Imperial fault were started (Sharp *et al.*, 1982). A secondary fault, the Brawley fault, showed primarily vertical offset of much smaller amplitude than the offsets on the Imperial fault (Sharp *et al.*, 1982). The fault traces on which measurable offsets were recorded are shown in Figure 1. The epicenter is

about 2.0 km south of the United States-Mexico border but the southernmost observed surface offsets were recorded about 5.0 km north of the international border. From the location of the epicenter and the places where surface slip was measured, it is likely that the rupture propagated primarily northward from the epicenter, although Olson and Apsel (1982) give evidence for some southward propagation of the rupture at depth. Shown in Figure 16A is the right-lateral offset on the Imperial fault about 160 days after the earthquake. An almost logarithmic increase with time in the total offset followed the coseismic offset (Sharp *et al.*, 1982) similar to measurements after the 1966 Parkfield earthquake (Smith and Wyss, 1968). This postseismic slip after the main shock could be due to the release of near-surface strain concentrated by larger slip at greater depth (Archuleta and Day, 1980).

Vertical offsets were found along the entire surface break, with the largest offsets near the northern terminus of the Imperial fault (Sharp *et al.*, 1982) (Figure 16B). The occurrence of vertical offsets at the northern end of the Imperial fault during past earthquakes is suggested from a prominent scarp with the west side upthrown by about 8 m relative to the east side (Sharp and Lienkaemper, 1982). Even though the Imperial fault is almost exclusively strike-slip, the vertical offsets are expected when one considers that the fault plane terminates at the northern end and it intersects the free surface (Chinnery, 1961).

The line of strong motion accelerographs E01 to E13 crosses the Imperial fault about 25 km north of the epicenter. This would place stations E06 and E07 about 22 km north of the international border. At the point on the Imperial fault closest to E06 and E07, the horizontal slip was 21 cm, from measurements made about 3 days after the main shock; at the same time, the maximum horizontal slip was about 62 cm at a point 6 km north of the border (Sharp *et al.*, 1982). Although the amplitude of the horizontal slip increased with time, the distribution of slip measured within several days after the earthquake is very similar to the slip distribution shown in Figure 16A. An important feature of this slip distribution is that the continuous break extends at least 9 km north of the stations E06 and E07. In addition to the horizontal offsets, the vertical offsets measured about 10 days after the main shock show a distribution along strike almost identical to that shown in Figure 16B. The maximum vertical offset was 36 cm at a point about 4 km north of E06 and E07. Based on the observed distribution of vertical offsets, I infer that the end of the dynamic faulting was also 4 km north of the strong motion stations (Chinnery, 1961). Regardless of the exact end of the faulting, the distribution of static measurements definitely supports the idea that the rupture passed by E06 and E07 during the main shock.

Given that the Imperial Valley is not a uniform half-space, there is an open-ended question as to how much information about the seismic moment, static stress drop, and strain drop can be deduced from the static offsets. As I progress in this discussion of these source parameters, it will become clear that the uncertainty in the estimates of these parameters depends upon one's knowledge of the slip distribution at depth. The determination of a detailed slip distribution such as that given by Hartzell and Helmberger (1982) is beyond the scope of this paper. Lacking this, however, one can determine lower bounds which are useful in discussing some of the gross features of the faulting.

First I estimate the seismic moment  $M_0$  from the horizontal slip. The seismic moment can be written  $M_0 = \mu A \bar{s}$  where  $\mu$  is the shear modulus,  $\bar{s}$  is the average slip, and  $A$  is the total area of the fault. In order to approximate this formula in a

vertically varying medium, a number of assumptions must be made. The first assumption is that the depth of faulting extends only to 10 km. Historically, seismicity on the Imperial fault has been located to depths of 9 to 11 km (Fuis *et al.*, 1978). Two aftershocks within minutes of the main shock were located on the Imperial fault south of stations E06 and E07; the  $M_L$  3.8 aftershock has a depth around 5 km and the  $M_L$  5.2 has a depth around 10 km (C. Mueller, personal communication). Furthermore, the main shock hypocenter is at 8 km (Archuleta, 1982). Although no direct evidence places a limit on the depth of faulting, 10 km is a reasonable value. For subsequent calculations, I will break this depth interval into two 5 km wide subintervals corresponding to the sediments and basement. A rough estimate of the length of faulting in the sediments and basement can be obtained from Figure 16. For the upper 5 km, I take the length of observed surface rupture, 30 km, and for the deeper 5 km I choose the distance from the epicenter to the most distant surface rupture, 37.5 km, presuming no southward rupture from the epicenter. In the sediments, a mean  $V_s^2$  of  $3.3 \text{ km}^2/\text{sec}^2$  and a density of  $2.25 \text{ gm/cm}^3$  from the gravity modeling of Fuis *et al.* (1982) yield a mean shear modulus of  $7.4 \times 10^{10} \text{ dyne-cm}^{-2}$ , while in the basement, I use a mean shear velocity of 3.2 km/sec and density of  $2.6 \text{ gm/cm}^3$ . Not knowing how slip varies with depth, I first assume that the average surface slip of 40.5 cm is constant over the entire fault. Since slip probably increases with depth, this assumption leads to a lower bound on moment. With these assumptions, I obtain a moment of about  $2.5 \times 10^{25} \text{ dyne-cm}$ , with the sediments contributing about  $0.5 \times 10^{25} \text{ dyne-cm}$  and the basement contributing the remainder. Even though this may be a crude estimate of the true seismic moment, this analysis indicates that the deeper part of the fault may have a significantly greater contribution to the low-frequency near-source ground motion than the shallow part of the fault due to its larger area and shear modulus.

Comparing this lower bound estimate of seismic moment with that determined by other investigators, it is 2.4 times smaller than the estimate made by Kanamori and Regan (1982) using surface waves and 3.6 times smaller than the estimate made by Wyatt (1980) using strain steps at Pinon Observatory about 130 km from the Imperial fault. Although my estimates of the length and depth of faulting may be imprecise, it is unlikely that one could realistically change these variables to account for a factor of 2 or 3. Although the shear moduli depend on the S-wave velocity structure, the major contribution to the seismic moment comes from the nearly homogeneous layer at depth where the assumed S-wave velocity is a rather typical value for crustal material. Some error in the average modulus for the shallow part of the fault may exist; however, it is unlikely to account for a factor of 2 or 3. The most likely source of the discrepancy between the estimate of seismic moment determined from the static slip and the far-field estimates is the assumption that the average slip of 40.5 cm at the surface is valid at all depths. For example, one can match the observed far-field seismic moment by allowing the average slip in the basement to be 120 cm while holding average sediment slip to 40.5 cm, or alternately by allowing average slip to be 105 cm over the entire fault. Thus, it is clear that if the surface slip reflects slip in the shallow part of the fault, then the deeper part of the fault is likely to play a much more significant role in the near-source dynamic ground motion.

Although the average surface slip measurements provide an estimate of the seismic moment that is an average property of the faulting, there is greater uncertainty about the usefulness of a static stress drop inferred from the average surface slip. As demonstrated in a theoretical study by Mavko (1982), different

faults with the same average moment and the same average stress drop can have stress variations that differ by an order of magnitude from one fault to the next. These stress variations arise from the fact that it is the derivative of the slip along the fault plane that determines the local value of stress (Bilby and Eshelby, 1969; Mavko, 1982). Bearing in mind that large stress variations may exist and that the effect of such variations can be important in determining the near-source particle motions (Boatwright, 1982; Hartzell and Helmberger, 1982; McGarr, 1982), the average static stress drop has its primary utility for comparison purposes with other large earthquakes whose stress drops are based on a similar analysis. The average static stress drop for a long strike-slip earthquake which breaks the surface in a uniform half-space is related to the average slip by  $\Delta\sigma = 2 \mu \bar{s} / \pi W$  (Kanamori and Anderson, 1975) where  $\Delta\sigma$  is the average static stress drop,  $\mu$  is the shear modulus,  $\bar{s}$  is the average slip, and  $W$  is the width of faulting for the given average slip. Rather than use the average surface slip to estimate the static stress drop, I use the average value of 105 cm and width of 10 km which is consistent with the far-field seismic moment of Kanamori and Regan (1982). Substituting an average  $V_s^2$  of 6.78 km<sup>2</sup>/sec<sup>2</sup> and an average density of 2.5 gm/cm<sup>3</sup> into the expression for  $\Delta\sigma$ , I find an average static stress drop of 11 bars. This estimate is consistent with the static stress drop of 5 to 10 bars determined by Hartzell and Helmberger (1982). However, one can estimate the static stress drop in another way. Consider the hypothetical example in which the upper 5 km has a average displacement of 40.5 cm, and the lower 5 km has an average displacement of 120 cm. If I approximate the average stress drop for the two-layer model as  $\Delta\sigma = (\mu_1 s_1 + \mu_2 s_2) / (W_1 + W_2)$ , where the subscript 1 refers to variables in the upper 5 km of the fault and the subscript 2 refers to variables in the lower 5 km of the fault, then I find that  $\Delta\sigma = 39$  bars. While only approximate, this estimate is considerably higher than the previous estimate. Considering that the maximum particle velocities were on the order of 100 cm/sec and the maximum horizontal accelerations were on the order of 0.5 to 0.8 g, this estimate of 39 bars for the static stress drop may seem more likely than the estimate of 11 bars if we consider Brune's (1970) source model as an indicator of the amplitude of the near-source ground motion for a given stress drop. A better estimate of the average stress drop must be deferred to a later paper in which modelling of the near-source particle velocities can better define the slip distribution with depth.

Although the static stress drop estimate of 11 bars may be a lower bound on the actual average stress drop, this lower bound has important implications about the strain released during the main shock. Using Hooke's law, the strain drop is  $\Delta\epsilon = \Delta\sigma / 2\mu$  where  $\Delta\sigma$  is the average static stress drop and  $\mu$  the average shear modulus. Using  $1.7 \times 10^{11}$  dyne-cm<sup>-2</sup> for the average shear modulus and 11 bars for the average static stress drop, a lower bound for the strain drop is 32  $\mu$ strain. If one assumes that the 1940 El Centro earthquake ( $M_S = 7.1$ ) relieved all of the tectonic strain when it ruptured this segment of the fault and a uniform shear strain buildup ensued at a rate of 0.2  $\mu$ strain per year (Savage and Burford, 1970; Savage *et al.*, 1981) for 39 yr, the accumulated shear strain would be only 8  $\mu$ strain, 4 times smaller than the lower bound estimate for the strain drop of the 1979 main shock. Considering that the average shear strain rate was 0.2  $\mu$ strain for the period 1941 to 1967 (Savage and Burford, 1970) and 0.25  $\mu$ strain for the period 1972 to 1978.9 (Savage *et al.*, 1981), the assumption of strain accumulation at 0.2  $\mu$ strain per year seems reasonable because the strain rate declined in the period 1954 to 1967 (Thatcher, 1979), presuming that nothing unusual occurred in the period 1967 to 1971. The probable explanation for this discrepancy is that the 1940 earthquake did not relieve

all the tectonic strain on the northern part of the Imperial fault. Clear evidence of this possibility is the distribution of slip following the 1940 earthquake [Figure 16 of Hartzell and Helmberger (1981)] which shows over 250 cm of slip from the international border south but only about 80 cm of slip on the same part of the Imperial fault that ruptured in the 1979 earthquake. Even if the 1979 surface slip were added to the 1940 slip, the slip deficit on the northern part of the Imperial fault would still be about 2.5 times smaller than the slip that occurred for 20 km south of the United States-Mexico border during the 1940 earthquake. It is possible that south of the United States-Mexico border, the slip that occurred during the 1940 event better reflects the slip at depth, whereas based on the earlier calculations of the seismic moment, the surface slip in 1979 could be a factor of 2 or 3 smaller than the slip at depth. Another possibility is that there is still enough residual strain on the northern part of the Imperial fault for another earthquake equal to or larger than the 1979 event at any time.

#### ACKNOWLEDGMENTS

This paper has benefited from conversations and criticisms from Dave Boore, Steve Hartzell, Gary Fuis, Gary Mavko, and Walter Mooney, who suggested the *PP* hypothesis. Larry Porter of CDMG provided us with the state's free-field data, and Robert Sharp and James Lienkaemper gave us their unpublished static-slip measurements. I thank Allen Olson for an early copy of his DWFE code, Edward Cranswick, who organized and plotted the data and devised the polarization plots, and Paul Spudich, who helped calculate the theoretical seismograms shown in this paper. This work was supported by the Office of Nuclear Regulatory Research, U.S. Nuclear Regulatory Commission.

#### REFERENCES

- Anderson, J. G. and P. G. Richards (1975). Comparison of strong ground motion from several dislocation models, *Geophys. J.* **42**, 347-373.
- Archuleta, R. J. (1982). Hypocenter for the 1979 Imperial Valley, California, earthquake, *Geophys. Res. Letters* **9**, 625-628.
- Archuleta, R. J. and G. A. Frazier (1978). Three-dimensional numerical simulations of dynamic faulting in a half-space, *Bull. Seism. Soc. Am.* **70**, 541-572.
- Archuleta, R. J., P. Spudich, and A. Olson (1979). Synthetic seismogram studies of an aftershock of the 1979 Imperial Valley, California, earthquake, *Earthquake Notes* **50**, 50.
- Archuleta, R. J. and S. M. Day (1980). Dynamic rupture in a layered medium: the 1966 Parkfield earthquake, *Bull. Seism. Soc. Am.* **70**, 671-689.
- Ben-Menahem, A. (1962). Radiation of seismic body waves from a finite moving source in the earth, *J. Geophys. Res.* **67**, 345-350.
- Bilby, B. A. and J. D. Eshelby (1969). Dislocations and the theory of fracture, in *Fracture*, vol. 1, Academic Press Inc., New York.
- Boatwright, J. (1982). A dynamic model for far-field accelerations, *Bull. Seism. Soc. Am.* **72**, 1049-1068.
- Boore, D. M. and J. B. Fletcher (1982). The Imperial Valley earthquake of October 15, 1979. A preliminary study of selected aftershocks of the 1979 Imperial Valley earthquake from digital acceleration and velocity recordings, *U.S. Geol. Surv. Profess. Paper 1254* (in press).
- Brady, A. G., V. Perez, and P. N. Mork (1980). The Imperial Valley earthquake, October 15, 1979. Digitization and processing of accelerograph records, *U.S. Geol. Surv., Open-File Rept. 80-703*, 1-309.
- Brune, J. N. (1970). Tectonic stress and the spectra of seismic shear waves from earthquakes, *J. Geophys. Res.* **75**, 4997-5009.
- Brune, J. N., J. Prince, F. L. Vernon III, E. Mena, and R. S. Simons (1982). The Imperial Valley earthquake of October 15, 1979. Strong motion data recorded in Mexico during the October 15 mainshock, *U.S. Geol. Surv. Profess. Paper 1254* (in press).
- Bycroft, G. N. (1980). El Centro California differential ground motion array, *U.S. Geol. Surv., Open-File Rept. 80-919*, 1-13.
- Červený, V., I. A. Molotkov, and I. Psencik (1977). *Ray Method in Seismology*, Univerzita Karlova, Praha, 214 pp.
- Chavez, D., J. Gonzalez, A. Reyes, M. Medina, C. Duarte, J. N. Brune, F. Vernon III, R. Simons, L. K. Hutton, P. T. German, and C. E. Johnson (1982). The Imperial Valley earthquake of October 15,

1979. Main-shock location and magnitude determination using combined United States and Mexican data, *U.S. Geol. Surv. Profess. Paper 1254* (in press).
- Chinnery, M. A. (1961). The deformation of the ground around surface faults, *Bull. Seism. Soc. Am.* **51**, 355-372.
- Fuis, G. S., C. E. Johnson, and D. J. Jenkins (1978). Preliminary catalog of earthquakes in the northern Imperial Valley October 1977-December 1977, *U.S. Geol. Surv., Open-File Rept. 78-673*.
- Fuis, G. S., W. D. Mooney, J. H. Healy, G. A. McMechan, and W. J. Lutter (1982). The Imperial Valley earthquake of October 15, 1979. Crustal structure of the Imperial Valley region, *U.S. Geol. Surv. Profess. Paper 1254* (in press).
- Hartzell, S. and D. Helmberger (1982). Strong motion modeling of the Imperial Valley earthquake of 1979, *Bull. Seism. Soc. Am.* **72**, 571-596.
- Johnson, C. E. (1979). CEDAR—An approach to the computer automation of short-period local seismic networks; seismotectonics of the Imperial Valley of southern California, *Ph.D. Dissertation*, California Institute of Technology, Pasadena, California, 1-343.
- Julian, B. R., M. Zirbes, and R. Needham (1982). The Imperial Valley earthquake of October 15, 1979. The focal mechanism from the global digital seismograph network, *U.S. Geol. Surv. Profess. Paper 1254* (in press).
- Kanamori, H. and D. L. Anderson (1975). Theoretical basis of some empirical relations in seismology, *Bull. Seism. Soc. Am.* **65**, 1073-1095.
- Kanamori, H. and J. Regan (1982). The Imperial Valley earthquake of October 15, 1979. Long-period surface waves generated by the 1979 Imperial Valley earthquake, *U.S. Geol. Surv. Profess. Paper 1254* (in press).
- Kind, R. (1978). The reflectivity method for a buried source, *J. Geophys.* **44**, 603-612.
- Madariaga, R. (1977). High-frequency radiation from crack (stress-drop) models of earthquake faulting, *Geophys. J.* **51**, 625-651.
- Mavko, G. M. (1982). Easy computation of static stress drop, slip, and moment on two-dimensional heterogeneous faults, *Bull. Seism. Soc. Am.* **72**, 1499-1508.
- McGarr, A. (1982). Upper bounds on near-source peak ground motion based on a model of inhomogeneous faulting, *Bull. Seism. Soc. Am.* **72**, 1825-1841.
- McJunkin, R. D. and J. T. Ragsdale (1980). Compilation of strong-motion records and preliminary data from the Imperial Valley earthquake of 15 October 1979, Preliminary Report 26, California Division of Mines and Geology.
- McMechan, G. A. and W. D. Mooney (1980). Asymptotic ray theory and synthetic seismograms for laterally varying structures: theory and application to the Imperial Valley, California, *Bull. Seism. Soc. Am.* **70**, 2021-2035.
- Mueller, C. S. and D. M. Boore (1981). Site amplification at El Centro strong motion array station No. 6, *Earthquake Notes* **52**, 84.
- Niazi, M. (1982). Source dynamics of the 1979 Imperial Valley earthquake, from near-source observations of ground acceleration and velocity, *Bull. Seism. Soc. Am.* **72**, 1957-1968.
- Olson, A. H. (1982). Forward simulations and linear inversions of earthquake ground motions, *Ph.D. Thesis*, University of California, San Diego, 1-105.
- Olson, A. H. and R. J. Apsel (1982). Finite faults and inverse theory with applications to the 1979 Imperial Valley earthquake, *Bull. Seism. Soc. Am.* **72**, 1969-2001.
- Raugh, M. R. (1981). Procedures for analysis of strong-motion records, *Earthquake Notes* **52**, 17.
- Savage, J. C. and R. O. Burford (1970). Accumulation of tectonic strain in California, *Bull. Seism. Soc. Am.* **60**, 1877-1896.
- Savage, J. C., W. H. Prescott, M. Lisowski, and N. E. King (1981). Strain accumulation in southern California, 1973-1980, *J. Geophys. Res.* **86**, 6991-7001.
- Shannon and Wilson, Inc. and Agbabian Associates (1976). Geotechnical and strong motion earthquake data from U.S. accelerograph stations, I, Report NUREG-0029, prepared for the N.R.C.
- Sharp, R. V. and J. J. Lienkaemper (1982). The Imperial Valley earthquake of October 15, 1979. Pre- and post-earthquake near-field leveling across the Imperial and Brawley faults, *U.S. Geol. Surv. Profess. Paper 1254*. (in press).
- Sharp, R. V., J. J. Lienkaemper, M. G. Bonilla, D. B. Burke, B. F. Cox, D. G. Herd, D. M. Tiller, D. M. Morton, D. J. Ponti, M. J. Rymer, J. C. Tinsley, J. C. Yount, J. E. Kahle, E. W. Hart, and K. E. Sieh (1982). The Imperial Valley earthquake of October 15, 1979. Surface faulting in the central Imperial Valley, *U.S. Geol. Surv. Profess. Paper 1254*. (in press).
- Smith, S. W. and M. Wyss (1968). Displacement on the San Andreas fault subsequent to the 1966 Parkfield earthquake, *Bull. Seism. Soc. Am.* **58**, 1955-1973.
- Spudich, P. (1981). Frequency domain calculation of extended source seismograms, *EOS* **62**, 960.

- Spudich, P. and E. Cranswick (1982). Use of near-source seismic-array data to reveal details of the earthquake rupture process, *Earthquake Notes* 53, 39.
- Switzer, J., D. Johnson, R. Maley, and R. Matthiesen (1981). Western hemisphere strong motion accelerograph station list-1980, *U.S. Geol. Surv., Open-File Rept. 81-664*, 1-153.
- Thatcher, W. (1979). Horizontal crustal deformation from historic geodetic measurements in southern California, *J. Geophys. Res.* 84, 2351-2370.
- Wyatt, F. (1980). Theoretical and observed surface deformations due to a distant earthquake, *EOS* 61, 211.

U.S. GEOLOGICAL SURVEY  
OFFICE OF EARTHQUAKE STUDIES  
345 MIDDLEFIELD ROAD  
MENLO PARK, CALIFORNIA 94025

Manuscript received 19 March 1982